Annals of Nuclear Energy 122 (2018) 352–365

Contents lists available at ScienceDirect

Annals of Nuclear Energy

journal homepage: www.elsevier.com/locate/anucene

A comprehensive study on source terms in irradiated graphite spheres of HTR-10

Feng Xie [a], Hong Li [a], Xuegang Liu [a,*], Jing Chen [a], Chuan Li [a], Xiaotong Chen [a], Karl Verfondern [b]

[a] Institute of Nuclear and New Energy Technology, Collaborative Innovation Center of Advanced Nuclear Energy Technology, Key Laboratory of Advanced Reactor Engineering and Safety of Ministry of Education, Tsinghua University, Beijing 100084, China
[b] Research Center Juelich, Institute for Energy and Climate Research, Nuclear Waste Management and Reactor Safety (IEK-6), 52425 Juelich, Germany

ARTICLE INFO

Article history:
Received 5 December 2017
Received in revised form 10 August 2018
Accepted 21 August 2018

Keywords:
10MW high temperature gas-cooled reactor
Activation products
Fission products
Irradiated graphite spheres
Specific activity

ABSTRACT

With previously developed experimental methods which include the preparation and measurement process for the graphite sample, two new irradiated graphite spheres with surface γ dose rates of 51.00 μSv/h and 0.14 μSv/h from the reactor core of the 10 MW high temperature gas-cooled reactor (HTR-10) have been investigated experimentally. The total β counting rate, the β spectra and the γ spectra for each graphite sample of irradiated graphite spheres were recorded with a total α/β counting measuring apparatus, a liquid scintillation counter and a high-purity germanium detector connected to a multichannel analyzer, respectively. Combined with previous experimental data of two irradiated graphite spheres with surface γ dose rates of 25.10 μSv/h and 1.17 μSv/h, the types of key nuclides in the irradiated graphite sphere of HTR-10 were determined, which were H-3, C-14, Co-60, Cs-137, Eu-152 and Eu-154. The distributions for each nuclide in four irradiated graphite spheres were compared. The generation mechanisms of H-3, C-14, Co-60, Cs-137, Eu-152 and Eu-154 in the irradiated graphite sphere of HTR-10 were discussed and analyzed. Based on all the experimental data regarding impurities and uranium contamination in the matrix graphite of HTR-10 available, a sensitivity analysis was performed to explain the effect of impurities and uranium contamination on the specific activity of key nuclides in the graphite sphere. The influence of the neutron flux and the dwell time in the core on the specific activity of key nuclides was also considered. The differences of experimental specific activities among these irradiated graphite spheres were compared and explained. Current comprehensive studies on irradiated graphite spheres of HTR-10 can provide valuable information for the source term analysis, waste minimization and radiation protection of high temperature gas-cooled reactors (HTGRs).

1. Introduction

In the Generation IV Program, the very high temperature reactor (VHTR) has been identified as one of the six technologies for development as a next generation nuclear energy system (NERAC and GIF, 2002). Compared to the current high temperature gas-cooled reactor (HTGR), the VHTR is expected to supply electrical production with a high efficiency and provide versatility in process-heat generation or co-generation at a high temperature level. However, with respect to the safety assessment of VHTR, current reliable data about radionuclides including fission products and activation products in the primary circuit, especially in the reactor core is rather rare (Morris et al., 2008; Kissane, 2009). The relevant information can be derived from the operating experience and experiments on the high temperature gas-cooled reactors (HTRs). For a pebble bed core, the Arbeitsgemeinschaft Versuchsreaktor (AVR) in Germany had accomplished a series of experimental programs to study the radioactive source term and made up a knowledge base for understanding the behavior of fission products and activation products in HTGRs (Bäumer and Barnert, 1990; IAEA, 1997; IAEA, 2012).

After the decommissioning of AVR and the thorium high temperature reactor (THTR-300) in Germany, the 10 MW high temperature gas-cooled test reactor (HTR-10) is the only pebble bed reactor working in the world, which is the first gas-cooled pebble bed test reactor in China. It uses helium as the primary coolant and graphite as a moderator and reflector (Wu et al., 2002). The spherical fuel elements with 60 mm in diameter embedded tristructural-isotropic (TRISO) coated particles are adopted, which are composed of two parts: a fuel zone with 50 mm in diameter and a fuel-free shell of 5 mm in thickness (Tang et al., 2002). The

* Corresponding author.
E-mail address: liu-xg@mail.tsinghua.edu.cn (X. Liu).

https://doi.org/10.1016/j.anucene.2018.08.034
0306-4549/

HTR-10 attained first criticality in December 2000, realized full power operation at the beginning of 2003, and demonstrated several expected safety features of a pebble bed HTGR by July 2007 (Zhang et al., 2009). Then it was shut down and totally HTR-10 was operated about 225 equivalent full power days (EFPDs). In 2015, HTR-10 was restarted and operated at 2.9 MW for about 90 days (Wei et al., 2016). In order to obtain more valuable information about radioactive source terms in the primary circuit and reactor core, a series of experiments has been conducted in HTR-10, including: (1) measurement of the activity concentration of H-3 and C-14 in the primary coolant, (2) measurement of the concentration and particle distribution of radioactive dust in the primary circuit, and (3) measurement of the content and distribution of key nuclides in the irradiated graphite sphere from the reactor core (Xie et al., 2018, 2015, 2017; Liu et al., 2017; Li et al., 2017).

All fission products and activation products in a power plant come from the reactor core. To determine source terms in the core will be essential to study the transport behavior of fission products and activation products in the primary circuit and auxiliary systems. However, it is generally known to be difficult to determine the core temperature precisely with respect to the pebble bed reactor which might affect the performance of fuel elements. The direct investigation of irradiated fuel elements can lead to an extensive demand for experimental tools and radiation protection. For the initial core of a pebble bed reactor, a certain percentage of graphite spheres without fuel particles will be loaded into the core to balance the excess reactivity of the basically fresh fuels. From the transition core to the equilibrium core, graphite spheres will be gradually taken out. These graphite spheres have the same size and material of matrix graphite as fuel elements, and experienced nearly the same neutron flux and energy spectrum in the core. Since there are no fuel particles inside, the radiation level of the irradiated graphite sphere is rather low (usually about 1 μSv/h with the maximum less than 60 μSv/h), which makes it ideally suitable to obtain the radiological information about the pebble bed reactor core on one hand. On the other hand, to study the irradiated graphite sphere can provide unambiguous data about source terms in the nuclear graphite which has been widely used in HTGRs.

Liu et al. (2017) has established the analytical methodology to study the source term in the irradiated graphite sphere and determined the analytical procedure and parameters. Later, this analytical methodology was successfully applied to investigate the content and distribution of key nuclides in an irradiated graphite sphere of HTR-10 experimentally (Li et al., 2017). However, the key nuclides and corresponding specific activities exhibit distinct characters with different irradiated graphite spheres. In this paper, we will combine all the experimental data available from four graphite spheres irradiated in the reactor core of HTR-10 to compare the types, specific activities and distributions of key nuclides therein. Meanwhile we will gather all the information about impurities in the matrix graphite available to do a sensitivity analysis with the variation of neutron flux and dwell time in the core. The study whose results are presented here deals with the detailed investigation of four irradiated graphite spheres discharged from the reactor core during the shutdown stage of HTR-10 in 2014. As all graphite spheres loaded into the core were part of the initial core of HTR-10, their irradiation time of 225 EFPDs is precisely known. The fact that these four graphite spheres do not contain any coated fuel particles has the advantage that any measured radioactivity must originate from either natural contamination of the graphite material with uranium and impurities, respectively, or from activity that was transported with the cooling gas and deposited on the sphere surfaces, while an origin from the coated particles can be excluded. Therefore the measurements of surface contamination (such as Cs-137) provide valuable information on the overall fuel performance of the HTR-10 core, while other nuclides identified (such as Co-60) show the level of impurities in the graphitic material.

2. Experiment

The detailed experimental method and process can be found in Liu et al. (2017). Briefly to say, a mechanical method was adopted to obtain a cylindrical graphite stick sample through the center of the irradiated graphite sphere with a homemade drilling machine (SIEG SUPER X3, from Shanghai SIEG Machinery Co., Ltd). The graphite stick of 60 mm in length and 7 mm in diameter was used to prepare graphite powder samples at different radial positions of the graphite sphere. Fig. 1 shows the cylindrical graphite stick sample drilled from the irradiated graphite sphere.

As indicated earlier, the graphite powder samples were measured first with a total α/β analyzer (BH1216III, from CNNC Beijing Nuclear Instrument Factory). Then a high-purity germanium detector connected to a multichannel analyzer (GC3018 detector, from Canberra Company) was used to record the γ spectra of the solid sample. After that, the graphite powder samples were combusted sufficiently in a vessel (1180B, from Parr Instrument Company) and the exhaust gas was absorbed in NaOH solution. Finally, an automatic potentiometric titrator (809Titrando, from Metrohm Company) was applied to determine the carbon content in the liquid sample and the liquid scintillation counter (Quantulus 1220, from Perkin Elmer Company) was used to measure the β spectra of the liquid sample.

By now, four irradiated graphite spheres discharged from the reactor core of HTR-10 have been investigated experimentally. The experimental results of the first two graphite spheres have been presented in previous literatures (Liu et al., 2017; Li et al., 2017). In this article, all the experimental data available were considered for comparison and analysis. Table 1 lists the mass, the surface γ dose rate and the average total β counting rate per gram for the four irradiated graphite spheres, which were denoted as A, B, C and D for convenience.

Fig. 1. Cylindrical graphite stick sample drilled from the irradiated graphite sphere of HTR-10.

Table 1
The mass, the surface γ dose rate and the average total β counting rate per gram for four irradiated graphite spheres of HTR-10.

Graphite sphere	Mass (g)	Surface γ dose rate (μSv/h)	Average total β counting rate per gram (CPS/g)
A	~210*	25.10	92.55
B	210.95	1.17	11.64
C	200.33	51.00	197.16
D	196.03	0.14	0.34

* This value was estimated from the graphite sphere after drilling with considering the mass of the graphite stick.

3. Experimental results

For comparison, we plot the total β counting rate per gram, γ spectra, β spectra, and specific activity distribution of key nuclides of graphite spheres A and B together with the new data from graphite spheres C and D.

Fig. 2 exhibits radial distributions of the total β counting rate per gram in the four irradiated graphite spheres, which can provide qualitative aggregate activity information about the distribution of nuclides in the graphite matrix. The zero position stands for the center of the graphite sphere. When the whole graphite stick with 60 mm in length is measured, the relative position ranges from −30 mm to 30 mm, which is the case for graphite spheres B and C. When only half of the graphite stick was measured, the relative position ranges from 0 mm to 30 mm, which is the case for graphite spheres A and D. The average total β counting rates per gram in the four irradiated graphite spheres are 92.55 CPS/g (counts per second per gram), 11.64 CPS/g, 197.16 CPS/g and 0.34 CPS/g, respectively. Graphite sphere A and graphite sphere C present a rather uniform distribution. Graphite sphere D shows slightly larger values at the surface while graphite sphere B indicates an obviously larger value of total β counting rates per gram at the surface. The average total β counting rates per gram in irradiated graphite spheres are proportional to their surface γ dose rate values.

Fig. 3 presents the typical β spectrum of the liquid samples converted from the graphite samples at a radial position for three irradiated graphite spheres of HTR-10, including the samples at 29.0 mm, 14.6 mm, and 13.9 mm positions of irradiated graphite spheres A, B, and C, respectively. It clearly indicates the existence of H-3 and C-14 in the matrix graphite. In the graphite sphere D, there are counts from β rays of H-3 and C-14. However, the β emission is too weak to become visible in the spectra since the specific activities for the H-3 and C-14 in the irradiated graphite sphere D are 0.52 Bq/g and 0.78 Bq/g, respectively. Fig. 4 presents the typical

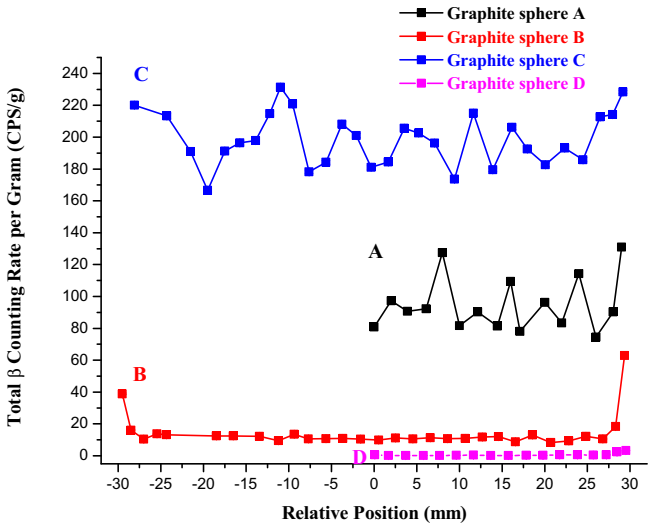

Fig. 2. Radial distribution of total β counting rate per unit gram in four irradiated graphite spheres of HTR-10.

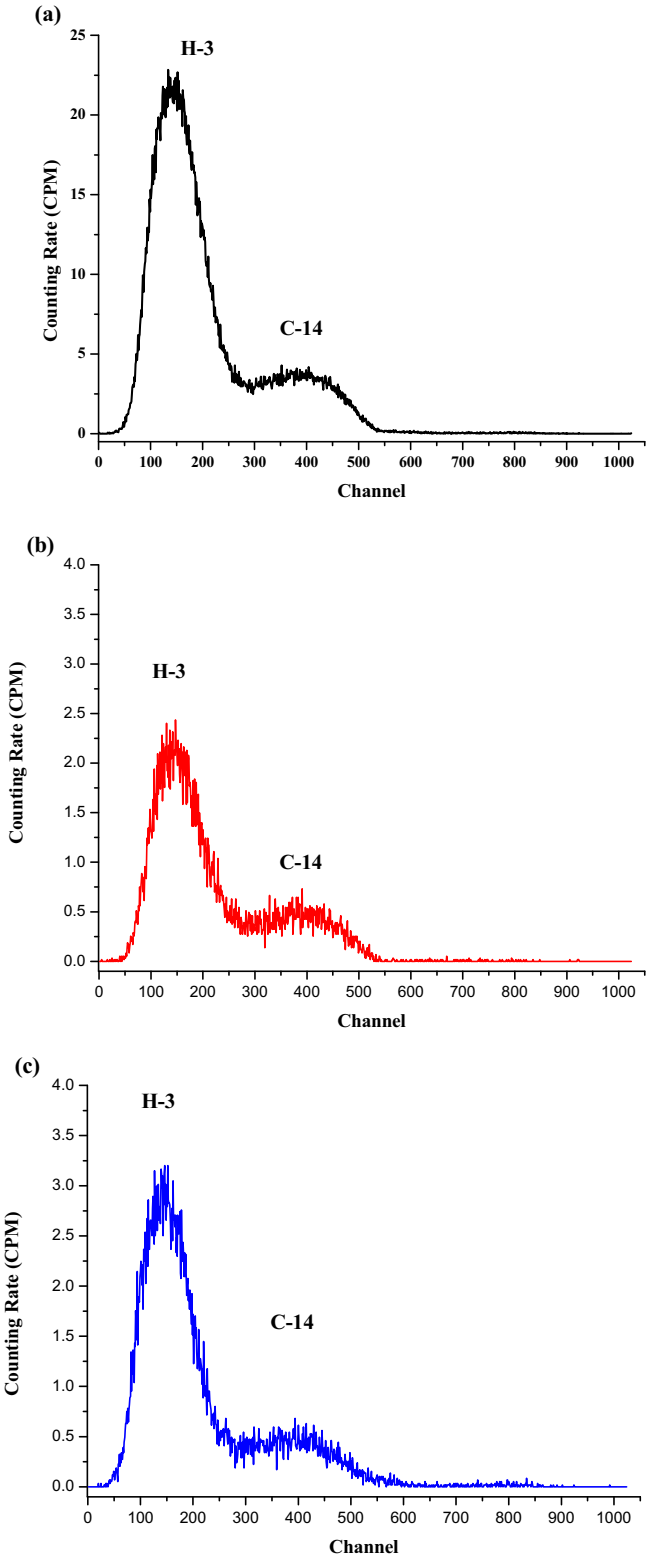

Fig. 3. Typical β spectrum of the liquid samples converted from the graphite samples at a radial position for three irradiated graphite spheres of HTR-10: (a) at 29.0 mm position of sphere A; (b) at 14.6 mm position of sphere B; (c) at 13.9 mm position of sphere C.

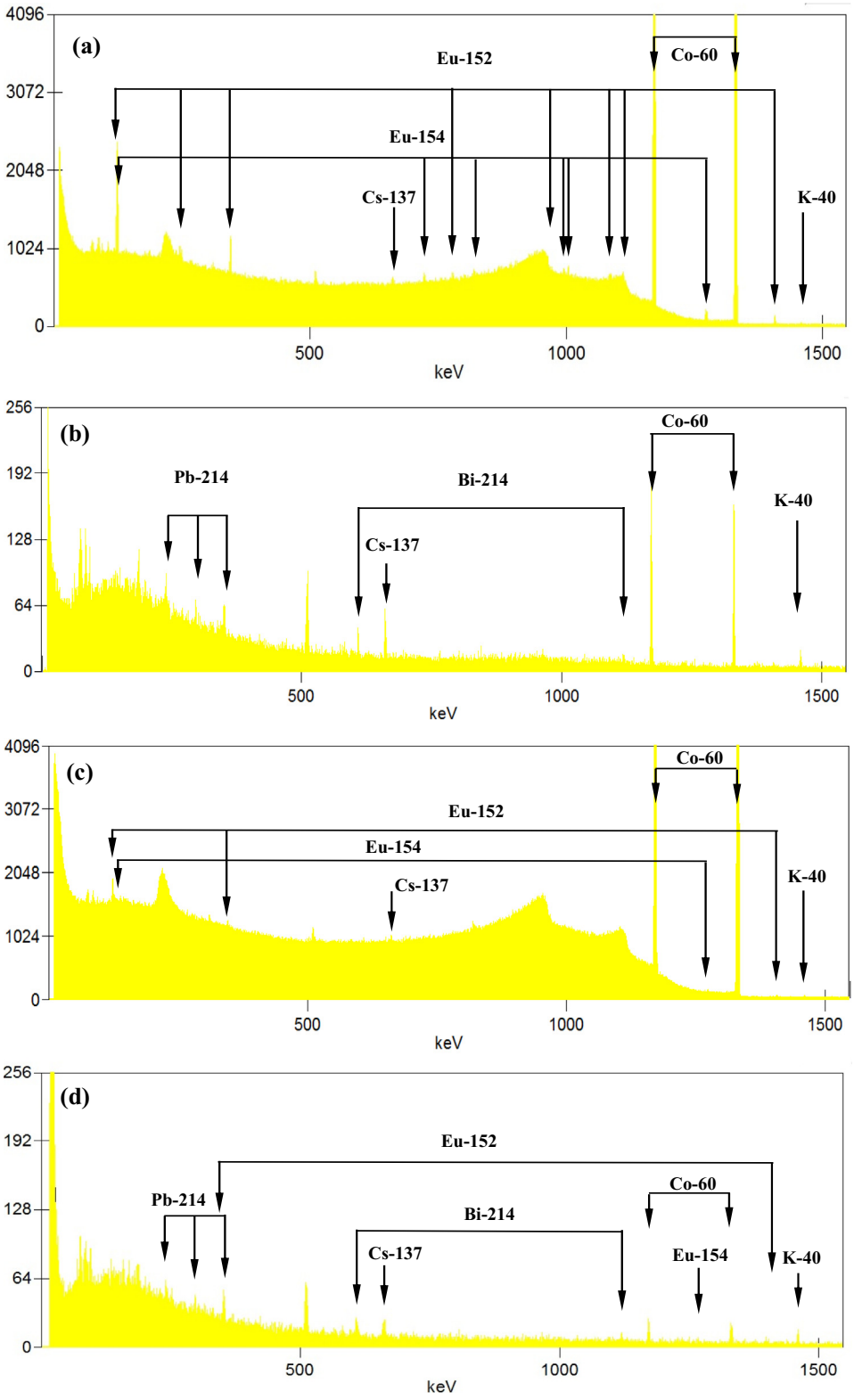

Fig. 4. Typical γ spectrum of the graphite samples at a radial position for four irradiated graphite spheres of HTR-10: (a) at 0.0 mm (center of the sphere) position of sphere A; (b) at 14.6 mm position of sphere B; (c) at 9.4 mm position of sphere C; (d) at 23.8 mm position of sphere D.

γ spectrum of the graphite samples at a radial position for four irradiated graphite spheres of HTR-10, including the samples at 0.0 mm (center of the sphere), 14.6 mm, 9.4 mm, and 23.8 mm positions of irradiated graphite spheres A, B, C, and D, respectively. The γ nuclides in the graphite material of irradiated graphite spheres of HTR-10 were explicitly identified. Table 2 lists the types of nuclides, and the corresponding half lives and peaks in the spectra for each irradiated graphite sphere. The isotopes K-40, Pb-214, and Bi-214 are natural radioactive nuclides, which means the measurement times are long enough to detect the radioactive nuclides

Table 2
Nuclides with corresponding half lives and peaks determined from the γ spectra of four irradiated graphite spheres of HTR-10.

Items	Nuclides	Half lives	Peaks (keV)
Graphite sphere A	Cs-137	30.17 a	661.7
	Eu-152	13.6 a	121.8, 244.7, 344.2, 778.8, 964.0, 1085.7, 1111.9, 1408.0
	Eu-154	8.8 a	123.0, 723.2, 873.1, 996.2, 1004.7, 1274.3
	Co-60	5.271 a	1173.2, 1332.6
	K-40	1.277E9 a	1460.8
Graphite sphere B	Cs-137	30.17 a	661.2
	Co-60	5.271 a	1173.2, 1332.6
	K-40	1.277E9 a	1460.8
	Pb-214	27.1 m	241.9, 295.2, 351.9
	Bi-214	19.9 m	609.3, 1120.2
Graphite sphere C	Cs-137	30.17 a	661.2
	Eu-152	13.6 a	121.8, 343.9, 1407.6
	Eu-154	8.8 a	122.8, 1273.6
	Co-60	5.271 a	1172.4, 1331.5
	K-40	1.277E9 a	1460.5
Graphite sphere D	Cs-137	30.17 a	661.2
	Eu-152	13.6 a	343.9, 1407.6
	Eu-154	8.8 a	1273.6
	Co-60	5.271 a	1172.4, 1331.5
	K-40	1.277E9 a	1460.5
	Pb-214	27.1 m	241.9, 295.2, 351.8
	Bi-214	19.9 m	608.6, 1120.1

in the graphite samples. Cs-137 and Co-60 exist in all four irradiated graphite spheres, which belong to the typical fission products and activation products in HTGRs. Their specific activities will be presented in Figs. 7 and 8 in the following text. The activities of Eu-152 and Eu-154 in the graphite spheres C and D are much smaller than those in the graphite sphere A, thus only the strongest peaks of Eu-152 and Eu-154 can be recognized in the γ spectra of graphite spheres C and D with a rather long measurement time. It was difficult to determine the specific activities and distributions of Eu-152 and Eu-154 in the graphite sphere C, but obviously they exist. However, in the graphite sphere B, no matter how long the measurement time was, no characteristic peaks of Eu-152 and Eu-154 appeared in the spectra.

Fig. 5 exhibits radial distributions of the H-3 specific activity in the four irradiated graphite spheres. The specific activities of H-3 in the interior of the graphite sphere exhibit nearly homogenous distribution and the average values are 7857.06 Bq/g, 96.20 Bq/g, 125.36 Bq/g, and 0.52 Bq/g, respectively, for the four spheres. However, at the surface, the H-3 shows a slightly higher concentration, which is clearly seen in the graphite spheres B, C and D. Fig. 6 exhibits radial distributions of the C-14 specific activity in the four irradiated graphite spheres. It looks like the distribution of C-14 in the graphite sphere is much more uniform than that of H-3. The average specific activities of C-14 in the interior are 1591.87 Bq/g, 25.20 Bq/g, 26.83 Bq/g, and 0.78 Bq/g, respectively, for the four irradiated graphite spheres. At the sphere surface, there is a somewhat higher concentration of C-14.

Fig. 7 presents radial distributions of Co-60 specific activities in the four irradiated graphite spheres. The specific activities of Co-60 in the interior of the graphite spheres show an even distribution and the average values are 1479.48 Bq/g, 26.35 Bq/g, 3324.45 Bq/g, and 4.00 Bq/g, respectively, for the four spheres. (Note that in the article of Liu et al. (2017), the efficiency factor for Co-60 between the count per second and the Bq is wrongly used, which is corrected in this paper.) Clearly, the specific activities of Co-60 at the surface are larger than the average values in the interior of graphite spheres A and B. However, the specific activity of Co-60 of graphite sphere C exhibits a relatively homogenous distribution

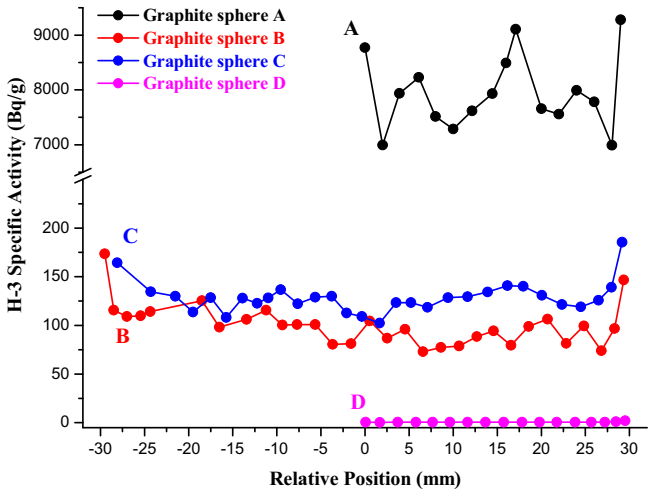

Fig. 5. Radial distributions of H-3 specific activity in four irradiated graphite spheres of HTR-10.

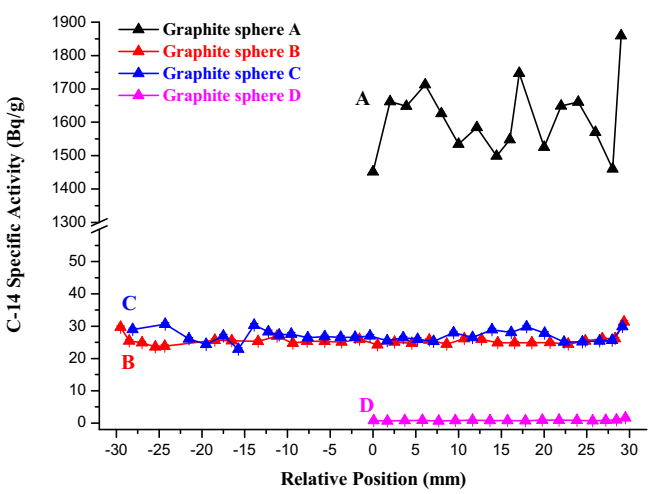

Fig. 6. Radial distributions of C-14 specific activity in four irradiated graphite spheres of HTR-10.

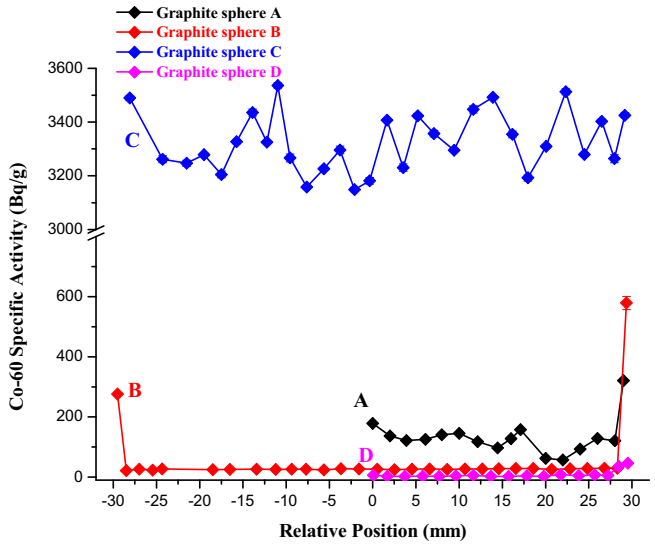

Fig. 7. Radial distributions of Co-60 specific activity in four irradiated graphite spheres of HTR-10.

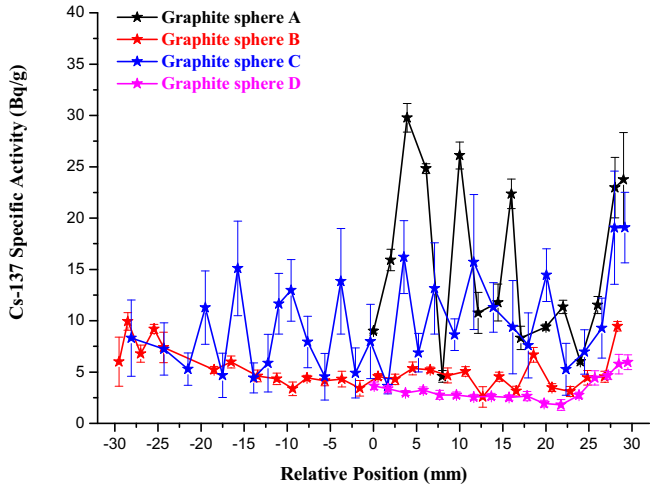

Fig. 8. Radial distributions of Cs-137 specific activity in four irradiated graphite spheres of HTR-10.

in the interior and at the surface. As for sphere D, the average specific activities of Co-60 are low with a slight increase at the surface.

Fig. 8 presents radial distributions of Cs-137 specific activities in the four irradiated graphite spheres. The specific activities of Cs-137 exhibit a nearly even distribution in the interior and at the surface of the spheres, of which the average values are 14.98 Bq/g, 5.15 Bq/g, 9.47 Bq/g, and 2.98 Bq/g, respectively.

In Liu et al. (2017), the distributions of the specific activities of Eu-152 and Eu-154 in the irradiated graphite sphere A have been presented, and the average values are 28.19 and 17.08 Bq/g, respectively. Since the specific activities of Eu-152 and Eu-154 in sphere B cannot be detected with current experimental instruments and the specific activities of Eu-152 and Eu-154 in sphere C are too small to determine the values, only the radial distributions of the specific activities of Eu-152 and Eu-154 in the irradiated graphite spheres A and D are presented in Figs. 9 and 10, respectively. Considering the uncertainty and the low specific activities, the radial distributions of Eu-152 and Eu-154 in the irradiated graphite spheres A and D can be thought nearly homogenous.

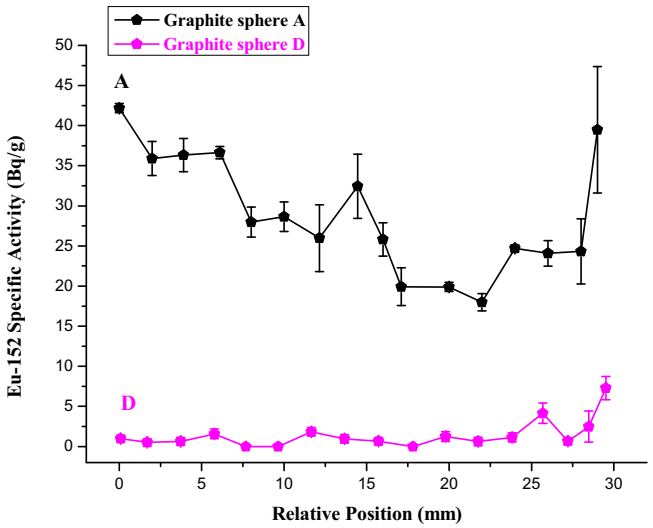

Fig. 9. Radial distributions of Eu-152 specific activity in the irradiated graphite spheres A and D of HTR-10.

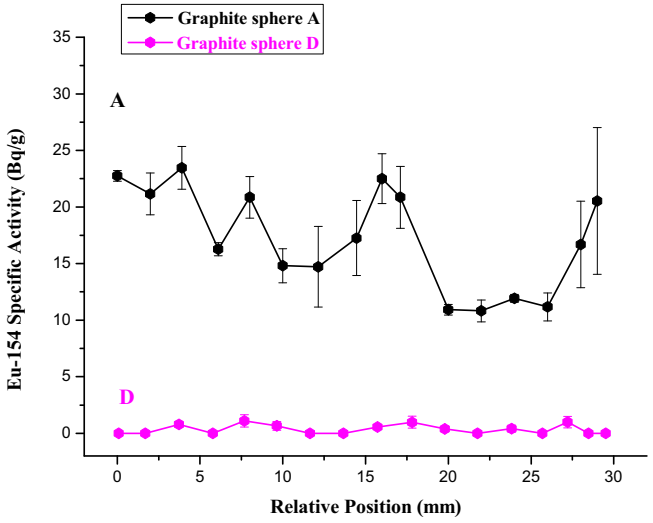

Fig. 10. Radial distributions of Eu-154 specific activity in the irradiated graphite spheres A and D of HTR-10.

4. Sensitivity analysis and calculations

The source terms in the irradiated graphite sphere of HTR-10 can be influenced by several factors, such as the content of impurities in the matrix graphite, the range of the neutron flux in the reactor core, the uranium contamination fraction in the graphite sphere, the dwell time for the graphite sphere in the core, etc. Table 3 lists the thermal and fast neutron fluence rate in the reactor core of HTR-10 at 225 EFPDs. In this section, we provide sensitivity analysis for key nuclides of H-3, C-14, Co-60, Cs-137, Eu-152 and Eu-154 to determine the dominant production source and crucial factors which can affect theoretical calculations on specific activities.

4.1. Source term analysis and specific activity calculations of H-3

The production mechanisms of H-3 in HTGRs have been determined in a series of studies (Gainey, 1976; Xu et al., 2017). Briefly said, H-3 can be generated by activation reactions of Li-6, Li-7 and

Table 3
Maximum value, average value, and minimum value of thermal and fast neutron flux in the reactor core at 225 equivalent full power operation days.

Item	Value
Maximum thermal neutron fluence rate in the core	4.16E+13 $cm^{-2}\cdot s^{-1}$
Average thermal neutron fluence rate in the core	3.45E+13 $cm^{-2}\cdot s^{-1}$
Minimum thermal neutron fluence rate in the core	2.93E+13 $cm^{-2}\cdot s^{-1}$
Maximum fast neutron fluence rate in the core	2.05E+13 $cm^{-2}\cdot s^{-1}$
Average fast neutron fluence rate in the core	1.44E+13 $cm^{-2}\cdot s^{-1}$
Minimum fast neutron fluence rate in the core	9.70E+12 $cm^{-2}\cdot s^{-1}$

B-10 in the irradiated graphite sphere. The specific activity of H-3 in the graphite sphere, $\bar{A}_T$, can be expressed as follows,

$$\bar{A}_T = \lambda_T \cdot \left(N_T^{G\_Li-6} + N_T^{G\_Li-7} + N_T^{G\_B-10}\right)/m \quad (1)$$

$$\frac{dN_T^{G\_Li-6}}{dt} = \sigma_{Li-6}\phi_{Th}N_{G\_Li-6} - \lambda_T N_T^{G\_Li-6} \quad (2)$$

$$\frac{dN_{G\_Li-6}}{dt} = -\sigma_{Li-6}\phi_{Th}N_{G\_Li-6} \quad (3)$$

$$\frac{dN_T^{G\_Li-7}}{dt} = \sigma_{Li-7}\phi_F N_{G\_Li-7} - \lambda_T N_T^{G\_Li-7} \quad (4)$$

$$\frac{dN_{G\_Li-7}}{dt} = -\sigma_{Li-7}\phi_F N_{G\_Li-7} \quad (5)$$

$$\frac{dN_T^{G\_B-10}}{dt} = \sigma_{(n,2\alpha)B-10}\phi_F N_{G\_B-10} + \sigma_{Li-7}\phi_F N_{Li-7}^{B-10} - \lambda_T N_T^{G\_B-10} \quad (6)$$

$$\frac{dN_{G\_B-10}}{dt} = -(\sigma_{(n,2\alpha)B-10}\phi_F + \sigma_{(n,\alpha)B-10}\phi_{Th}) \cdot N_{G\_B-10} \quad (7)$$

$$\frac{dN_{Li-7}^{B-10}}{dt} = \sigma_{(n,\alpha)B-10}\phi_{Th}N_{G\_B-10} - \sigma_{Li-7}\phi_F N_{Li-7}^{B-10} \quad (8)$$

where $N_T^{G\_Li-6}$, $N_T^{G\_Li-7}$, and $N_T^{G\_B-10}$ are the numbers of H-3 atoms generated by activation reactions of Li-6, Li-7, and B-10 in the graphite, respectively, N_{G_Li-6}, N_{G_Li-7}, and N_{Li-7}^{B-10} are the numbers of Li-6 atoms, Li-7 atoms, and Li-7 atoms produced by the B-10 activation in the graphite sphere individually, ϕ_{Th} and ϕ_F are the thermal and fast neutron fluence rate in the graphite sphere in the core ($cm^{-2}\cdot s^{-1}$) separately, λ_T is the decay constant of H-3 (s^{-1}), σ_{Li-6} is the cross section of the activation reaction of Li-6 (n, α) H-3 (b), σ_{Li-7} is the cross section of the activation reaction of Li-7 (n, nα) H-3 (b), $\sigma_{(n,2\alpha)B-10}$ is the cross section of the activation reaction of B-10 (n, 2α) H-3 (b), $\sigma_{(n,\alpha)B-10}$ is the cross section of the activation reaction of B-10 (n, α) Li-7 (b), and m is the mass of the graphite sphere of HTR-10 (g).

Table 4
Main Parameters for the calculation of H-3 in the irradiated graphite sphere of HTR-10.

Item	Value
Design value of Li mass fraction in the graphite sphere	0.3 ppm
Maximum Li mass fraction measured in the graphite sphere	0.001594 ppm
Average Li mass fraction measured in the graphite sphere	0.0004997 ppm
Minimum Li mass fraction measured in the graphite sphere	0.0002 ppm
Design value of B mass fraction in the graphite sphere	3 ppm
Maximum B mass fraction measured in the graphite sphere	1.831 ppm
Average B mass fraction measured in the graphite sphere	0.6749 ppm
Minimum B mass fraction measured in the graphite sphere	0.2014 ppm
Cross section of the activation reaction of Li-6 (n, α) H-3	942 b
Cross section of the activation reaction of Li-7 (n, nα) H-3	0.15 b
Cross section of the activation reaction of B-10 (n, 2α) H-3	0.05 b
Cross section of the activation reaction of B-10 (n, α) Li-7 (b)	3838 b

Table 5
Specific activity calculation results of H-3 with different parameters at 225 equivalent full power operation days.

Item		Specific activity of H-3 (Bq/g)		
		Flux		
		Maximum	Average	Minimum
Li (Li-6)	Design	8.62E+05	7.57E+05	6.72E+05
	Maximum	4.58E+03	4.02E+03	3.57E+03
	Average	1.44E+03	1.26E+03	1.12E+03
	Minimum	5.75E+02	5.05E+02	4.48E+02
Li (Li-7)	Design	1.19E+03	8.39E+02	5.65E+02
	Maximum	6.35E+00	4.46E+00	3.00E+00
	Average	1.99E+00	1.40E+00	9.41E−01
	Minimum	7.96E−01	5.59E−01	3.77E−01
B (B-10)	Design	1.31E+03	8.83E+02	5.70E+02
	Maximum	8.02E+02	5.39E+02	3.48E+02
	Average	2.96E+02	1.99E+02	1.28E+02
	Minimum	8.82E+01	5.93E+01	3.83E+01

Table 4 lists main parameters to calculate the specific activity of H-3 in the irradiated graphite sphere, including the Li and B mass fractions, and the cross sections of related activation reactions. In order to do a sensitivity analysis to determine key parameters which can affect the specific activity of H-3, several cases are considered for calculation, with different combinations of neutron fluence rate and mass fraction of impurities. The detailed calculation results are presented in Table 5. With the design values of Li mass fraction and B mass fraction, the total specific activity of H-3 in the irradiated graphite sphere of HTR-10 with 225 EFPDs can be as high as 7.59×10^5 Bq/g. While according to the measured values of Li and B mass fractions in the sampling batches of the graphite spheres, the calculated H-3 specific activities are much smaller. The H-3 produced by Li-7 activation is at least two orders of magnitude less than that by Li-6 activation, and the H-3 produced by B-10 activation is about one order of magnitude less than that by Li-6 activation. Therefore, the dominant source term of H-3 in the irradiated graphite sphere comes from the activation reaction of Li-6 in the graphite.

Fig. 11 presents calculation results of H-3 specific activity in comparison with average experimental values of H-3 in the four

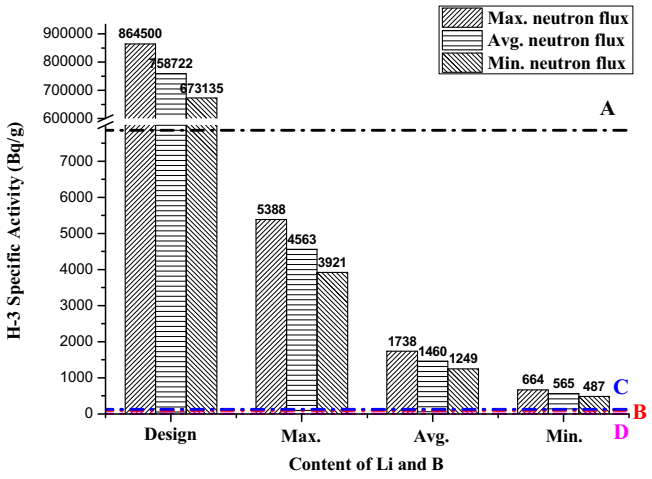

Fig. 11. Comparison of calculated H-3 specific activities based on different neutron fluxes (maximum, average and minimum) and different contents of Li and B (design, maximum, average and minimum) with average experimental values from the four irradiated graphite spheres of HTR-10.

irradiated graphite spheres. In the sampling batches of the graphite spheres, the measured maximum Li mass fraction, 0.001594 ppm, is much less than the design value, 0.3 ppm. On the other hand, the measured maximum B mass fraction, 1.831 ppm, is close to the design value of 3 ppm. Even so, the H-3 generated from the Li-6 activation is much larger than that from the B-10 activation. The control of the Li mass fraction in the graphite of HTR-10 can reduce the specific activity of H-3 in the irradiated graphite spheres effectively.

4.2. Source term analysis and specific activity calculations of C-14

In HTGRs, the generation of C-14 has been analyzed in several studies (Davis, 1977; Wichner and Dyer, 1980). In the irradiated graphite spheres, C-14 can be produced by activation reactions of C-13 and N-14 in the graphite. The specific activity of C-14 in the graphite spheres of HTR-10, $\bar{A}_{C-14}$, can be calculated as follows,

$$\bar{A}_{C-14} = \lambda_{C-14} \cdot (N_{C-14}^{G\_C-13} + N_{C-14}^{G\_N-14})/m \tag{9}$$

$$\frac{dN_{C-14}^{G\_C-13}}{dt} = \sigma_{C-13}\phi_{Th}N_{G\_C-13} - \lambda_{C-14}N_{C-14}^{G\_C-13} \tag{10}$$

$$\frac{dN_{G\_C-13}}{dt} = -\sigma_{C-13}\phi_{Th}N_{G\_C-13} \tag{11}$$

$$\frac{dN_{C-14}^{G\_N-14}}{dt} = \sigma_{N-14}\phi_{Th}N_{G\_N-14} - \lambda_{C-14}N_{C-14}^{G\_N-14} \tag{12}$$

$$\frac{dN_{G\_N-14}}{dt} = -\sigma_{N-14}\phi_{Th}N_{G\_N-14} \tag{13}$$

where $N_{C-14}^{G\_C-13}$ and $N_{C-14}^{G\_N-14}$ are the numbers of C-14 atoms generated by activation reactions of C-13 and N-14 in the graphite sphere, respectively, N_{G_C-13} and N_{G_N-14} are the numbers of C-13 atoms and N-14 atoms in the graphite sphere individually, σ_{C-13} is the cross section of the activation reaction of C-13 (n, γ) C-14 (b), σ_{N-14} is the cross section of the activation reaction of N-14 (n, p) C-14 (b), and λ_{C-14} is the decay constant of C-14 (s^{-1}).

Table 6 lists the main parameters for the calculation of C-14 source term in the irradiated graphite sphere of HTR-10. The designed C-13 mass fraction in the graphite are adopted with natural abundance. Since there are no measured N content data in the matrix graphite of HTR-10 available, the N mass fractions in the matrix graphite determined from the AVR graphite sphere are used in the calculation (Wenzel et al., 1979). The calculation results of specific activities of C-14 are provided in Table 7 considering 225 EFPDs. The C-14 produced from the C-13 activation is about 1.03×10^3 Bq/g with the average neutron fluence rate, and does not change much with the variation of neutron flux. However, the contribution from the N-14 activation can greatly affect the total specific activity of C-14 in the irradiated graphite sphere.

Table 6
Main parameters for the calculation of C-14 in the irradiated graphite sphere of HTR-10.

Item	Value
Maximum N mass fraction in the graphite sphere	30 ppm
Average N mass fraction in the graphite sphere	15 ppm
Minimum N mass fraction in the graphite sphere	1 ppm
Cross section of the activation reaction of C-13 (n, γ) C-14	9E−4 b
Cross section of the activation reaction of N-14 (n, p) C-14	1.82 b

Table 7
Specific activity calculation results of C-14 with different parameters at 225 equivalent full power operation days.

Item		Specific activity of C-14 (Bq/g)		
		Flux		
		Maximum	Average	Minimum
C-13	Design	1.24E+03	1.03E+03	8.75E+02
N (N-14)	Maximum	7.25E+03	6.01E+03	5.11E+03
	Medium	3.62E+03	3.01E+03	2.55E+03
	Minimum	2.42E+02	2.00E+02	1.70E+02

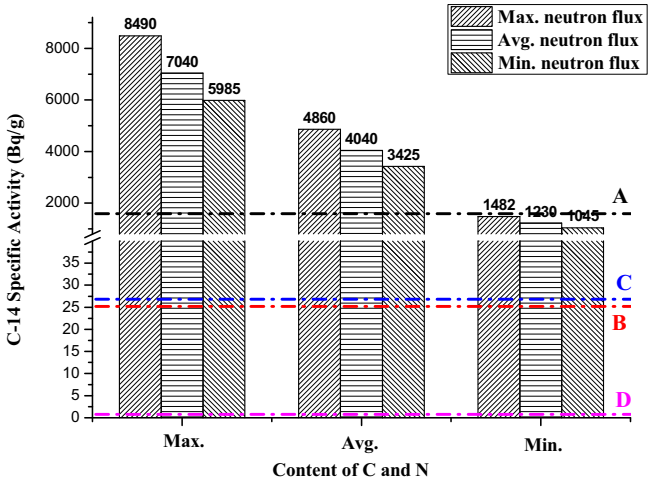

Fig. 12. Comparison of calculated C-14 specific activities based on different neutron fluxes (maximum, average and minimum) and different contents of C (design) and N (maximum, average and minimum) with average experimental values from the four irradiated graphite spheres of HTR-10.

Fig. 12 presents calculation results of C-14 specific activity in comparison with average experimental values of C-14 measured in the four irradiated graphite spheres indicating a little higher theoretical values than the experimental values even with the adoption of minimum values of neutron flux and impurities. The detail calculation results about the specific activities of C-14 in the graphite sphere can be found in Table 7. One possible reason is that the content of impurities in different batches of graphite spheres are distinctive, and there may exist much lower contents of impurities in some batches of graphite spheres. The other possible reason may be the uncertainty of operational historical and circulation route of spheres in the reactor core.

4.3. Source term analysis and specific activity calculations of Co-60

In HTGRs, Co-60 is a typical activation product which can be generated by the activation reactions of Co-59 and Ni-60 (Wang et al., 2015). The specific activity of Co-60 in an irradiated graphite sphere, $\bar{A}_{Co-60}$, can be expressed as follows,

$$\bar{A}_{Co-60} = \lambda_{Co-60} \cdot \left(N_{Co-60}^{G\_Co-59} + N_{Co-60}^{G\_Ni-60}\right)/m \tag{14}$$

$$\frac{dN_{Co-60}^{G\_Co-59}}{dt} = \sigma_{Co-59}\phi_{Th}N_{G\_Co-59} - \lambda_{Co-60}N_{Co-60}^{G\_Co-59} \tag{15}$$

$$\frac{dN_{G\_Co-59}}{dt} = -\sigma_{Co-59}\phi_{Th}N_{G\_Co-59} \tag{16}$$

$$\frac{dN_{Co-60}^{G\_Ni-60}}{dt} = \sigma_{Ni-60}\phi_{F}N_{G\_Ni-60} - \lambda_{Co-60}N_{Co-60}^{G\_Ni-60} \tag{17}$$

$$\frac{dN_{G\_Ni-60}}{dt} = -\sigma_{Ni-60}\phi_F N_{G\_Ni-60} \quad (18)$$

where $N_{Co-60}^{G\_Co-59}$ and $N_{Co-60}^{G\_Ni-60}$ are the numbers of Co-60 atoms generated by activation reactions of Co-59 and Ni-60 in the graphite sphere, respectively, N_{G_Co-59} and N_{G_Ni-60} are the numbers of Co-59 atoms and Ni-60 atoms in the graphite sphere individually, σ_{Co-59} is the cross section of the activation reaction of Co-59 (n, γ) Co-60 (b), σ_{Ni-60} is the cross section of the activation reaction of Ni-60 (n, p) Co-60 (b), and λ_{Co-60} is the decay constant of Co-60 (s^{-1}).

Table 8 lists main parameters for the calculation of Co-60 source terms in the irradiated graphite sphere of HTR-10. With the measured Co mass fractions, the measured and designed Ni mass fractions, and the maximum, average, and minimum neutron fluxes, the calculation results of specific activities of Co-60 considering 225 EFPDs are provided in Table 9. If we assume the designed Co mass fraction to be the same as the Ni mass fraction in the matrix graphite, the Co-60 generated from the Ni-60 activation will be three orders of magnitude less than that from the Co-59 activation with the same neutron flux and corresponding mass fraction. Obviously, the content of Co-59 in the matrix graphite plays a crucial role in the specific activity of Co-60 in the irradiated graphite sphere.

Fig. 13 exhibits calculation results of Co-60 specific activity in comparison with average experimental values of Co-60 measured in the four irradiated graphite spheres which indicate that calculation results agree well with the experimental values.

4.4. Source term analysis and specific activity calculations of Cs-137

Cs-137, which is a typical fission product in HTGRs, was determined to come from the uranium contamination in the matrix graphite (Li et al., 2017). The uranium contamination has two sources: the natural uranium contamination of the matrix material and the defective coated particles from the manufacturing process. For the four spheres investigated here, of course, only the natural uranium contamination applies. In this paper, we deduce the specific activity of Cs-137 in the irradiated graphite sphere, $\bar{A}_{Cs-137}$, according to the thermal power history of the reactor, which can be calculated as follows,

$$\bar{A}_{Cs-137} = \lambda_{Cs-137}\left(\sum_X N_{Cs-137}^{G\_X}\right)/m \quad (19)$$

$$\frac{dN_{Cs-137}^{X}}{dt} = k\cdot\frac{P_{th}}{g}\cdot y_X\cdot f_X - \lambda_{Cs-137}\cdot N_{Cs-137}^{X} \quad (20)$$

where $N_{Cs-137}^{G\_X}$ is the number of Cs-137 atoms generated by fission of the nuclide X in the irradiated graphite sphere of HTR-10 which is the fissile nuclide of U-235 here, λ_{Cs-137} is the decay constant of Cs-137, k is the fraction of the uranium contamination in the graphite sphere, P_{th} is the thermal power of the reactor (MW), y_x is the average yield of Cs-137 from fission of the nuclide X, f_X is the fission fraction of the nuclide X, and g is the energy released per fission (MW·s).

Table 10 presents the estimated fraction of natural U-235 in the matrix graphite to the U-235 in a fuel element and the measured natural uranium contamination fraction in the graphite sphere. Assuming the irradiated graphite spheres experienced 225 EFPDs in the reactor core, the specific activities of Cs-137 are calculated as 26.6 Bq/g and 3.09 Bq/g, respectively, on the basis of the estimated and measured natural U-235 fraction in the matrix graphite in a fuel element and in a graphite sphere individually. However, the specific activity of Cs-137 in the matrix graphite does not change much with varying the dwell time in the core. Thus, the crucial factor on the specific activity of Cs-137 in the irradiated graphite sphere lies in the natural uranium contamination fraction in the graphite.

Fig. 14 exhibits calculation results of Cs-137 specific activity in comparison with average experimental values measured in the four irradiated graphite spheres indicating that the calculation results agree well with the experimental values.

4.5. Source term analysis and specific activity calculations of Eu-152

Eu-152 can be produced as a fission product and also by neutron activation in the nuclear reactor (Niese and Gleisberg, 1996; Lahiri et al., 2005). Therefore it can be found in spent fuel and in

Table 8
Main Parameters for the calculation of Co-60 in the irradiated graphite sphere of HTR-10.

Item	Value
Maximum Co mass fraction measured in the graphite sphere	0.02698 ppm
Average Co mass fraction measured in the graphite sphere	0.006483 ppm
Minimum Co mass fraction measured in the graphite sphere	0.0002 ppm
Design value of Ni mass fraction in the graphite sphere	4 ppm
Maximum Ni mass fraction measured in the graphite sphere	0.2237 ppm
Average Ni mass fraction measured in the graphite sphere	0.04662 ppm
Minimum Ni mass fraction measured in the graphite sphere	0.006 ppm
Cross section of the activation reaction of Co-59 (n, γ) Co-60	37.18 b
Cross section of the activation reaction of Ni-60 (n, p) Co-60	0.13 b

Table 9
Specific activity calculation results of Co-60 with different parameters at 225 equivalent full power operation days.

Item		Specific activity of Co-60 (Bq/g)		
		Flux		
		Maximum	Average	Minimum
Co (Co-59)	Design	8.43E+05	7.00E+05	5.96E+05
	Maximum	5.69E+03	4.73E+03	4.02E+03
	Average	1.37E+03	1.14E+03	9.67E+02
	Minimum	4.21E+01	3.50E+01	2.98E+01
Ni (Ni-60)	Design	3.88E+02	2.73E+02	1.84E+02
	Maximum	2.17E+01	1.53E+01	1.03E+01
	Average	4.52E+00	3.18E+00	2.14E+00
	Minimum	5.82E−01	4.09E−01	2.76E−01

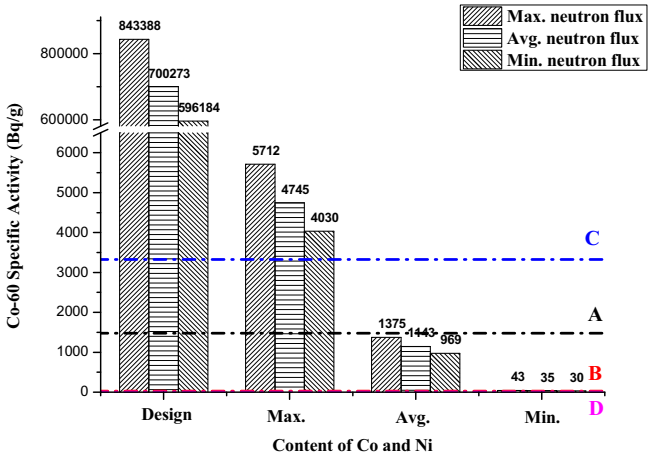

Fig. 13. Comparison of calculated Co-60 specific activities based on different neutron fluxes (maximum, average and minimum) and different contents of Co and Ni (design, maximum, average and minimum) with average experimental values from the four irradiated graphite spheres of HTR-10.

Table 10
Main Parameters for the calculation of Cs-137 in the irradiated graphite sphere of HTR-10.

Item	Value
Estimated fraction of natural U-235 in the matrix graphite to the U-235 in a fuel element	7.0×10^{-7}
Measured natural uranium contamination fraction in the graphite sphere	0.05 ppm
Fission fraction of Cs-137 produced from U-235	0.0631
Total number of fuel elements in the core	27,000

structure materials in the reactor core. In the graphite spheres of HTGRs, Eu-152 can be produced by fission reaction of uranium contamination in the matrix graphite. However, the yield of Eu-152 from fissile nuclide U-235 is much less than that of Cs-137 (Nichols et al., 2008). The dominant production source of Eu-152 in the irradiated graphite sphere of HTR-10 is the activation of Eu-151, which is one of the two natural isotopes of europium. The specific activity of Eu-152 in the irradiated graphite sphere of HTR-10, $\bar{A}_{Eu-152}$, can be deduced as follows,

$$\bar{A}_{Eu-152} = \lambda_{Eu-152} \cdot N_{Eu-152}^{G\_Eu-151}/m \tag{21}$$

$$\frac{dN_{Eu-152}^{G\_Eu-151}}{dt} = \sigma_{Eu-151}\phi_{Th}N_{G\_Eu-151} - \sigma_{Eu-152}\phi_{Th}N_{Eu-152}^{G\_Eu-151} - \lambda_{Eu-152}N_{Eu-152}^{G\_Eu-151} \tag{22}$$

$$\frac{dN_{G\_Eu-151}}{dt} = -\sigma_{Eu-151}\phi_{Th}N_{G\_Eu-151} \tag{23}$$

where $N_{Eu-152}^{G\_Eu-151}$ is the number of Eu-152 atoms generated by activation reactions of Eu-151 in the graphite sphere, N_{G_Eu-151} is the number of Eu-151 atoms in the graphite sphere, σ_{Eu-151} is the cross section of the activation reaction of Eu-151 (n, γ) Eu-152 (b), σ_{Eu-152} is the cross section of the activation reaction of Eu-152 (n, γ) Eu-153 (b), and λ_{Eu-152} is the decay constant of Eu-152 (s^{-1}).

Table 11 lists main parameters for the source term calculation of Eu-152 and Eu-154. Natural europium consists of Eu-151 and Eu-153 with approximately equal proportions, which can generate Eu-152 and Eu-154 by the neutron flux. Assuming the irradiated graphite spheres experienced 225 EFPDs in the reactor core, the specific activity of Eu-152 does not change much with variation of neutron flux. Since the measured Eu mass fraction values in the sampling batches of graphite spheres vary in a small range, from 0.0002 ppm to 0.0005 ppm, the calculated specific activity of Eu-152 changes very little.

Fig. 15 exhibits theoretical calculations of Eu-152 specific activity in comparison with average experimental values measured in the irradiated graphite spheres A and D. It seems that the measured Eu mass fraction values doesn't cover the irradiated graphite sphere A. This may be explained by large Eu mass fractions in the irradiated graphite sphere A compared to the measured values in sampling batches of graphite spheres.

Unlike the variation tendency of specific activities of H-3, C-14, and Co-60, the specific activity of Eu-152 becomes larger with the decrease of neutron flux. The reason is that the cross section of the activation reaction of Eu-152 (n, γ) Eu-153 is bigger than that of the activation reaction of Eu-151 (n, γ) Eu-152.

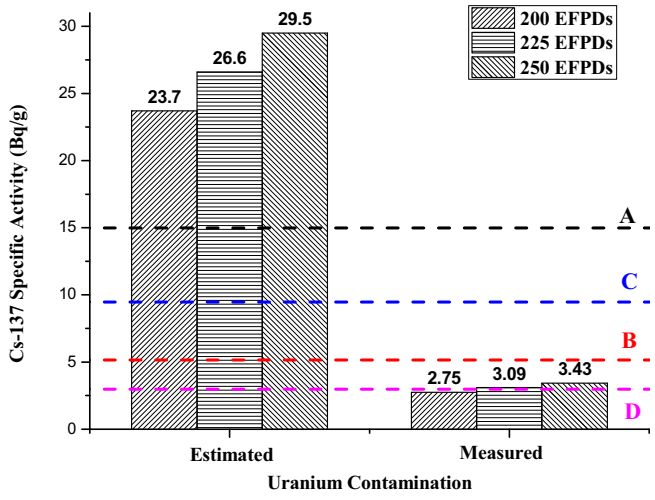

Fig. 14. Comparison of calculated Cs-137 specific activities based on different dwell times (200 EFPDs, 225 EFPDs and 250 EFPDs) in the core and natural uranium contamination (estimated and measured) with average experimental values from the four irradiated graphite spheres of HTR-10.

4.6. Source term analysis and specific activity calculations of Eu-154

Similar to Eu-152, Eu-154 can be produced by fission reactions and activation reactions (Smith et al., 1992; Niese and Gleisberg, 1996). The yield of Eu-154 from fissile reaction of U-235 is also much less than that of Cs-137 (Nichols et al., 2008). Therefore, in the irradiate graphite sphere of HTR-10, the Eu-154 is dominantly produced by the activation reaction of impurities in the graphite material. There are two generation mechanisms for Eu-154, which are (1) activation reaction of natural isotope of europium, Eu-153, which is Eu-153 (n, γ) Eu-154; (2) chain reaction of natural isotope of samarium, Sm-152, which is Sm-152 (n, γ) Sm-153 $\overset{\beta^-\ 46.284h}{\rightarrow}$ Eu-153 (n, γ) Eu-154 (Vimalnath et al., 2005). The specific activity of Eu-154 in the irradiated graphite sphere of HTR-10, $\bar{A}_{Eu-154}$, can be deduced as follows,

$$\bar{A}_{Eu-154} = \lambda_{Eu-154} \cdot \left(N_{Eu-154}^{G\_Eu-153} + N_{Eu-154}^{G\_Sm-152}\right)/m \tag{24}$$

$$\frac{dN_{Eu-154}^{G\_Eu-153}}{dt} = \sigma_{Eu-153}\phi_{Th}N_{G\_Eu-153} - \sigma_{Eu-154}\phi_{Th}N_{Eu-154}^{G\_Eu-153} - \lambda_{Eu-154}N_{Eu-154}^{G\_Eu-153} \tag{25}$$

Table 11
Main Parameters for the calculation of Eu-152 and Eu-154 in the irradiated graphite sphere of HTR-10.

Item	Value
Maximum Eu mass fraction measured in the graphite sphere	0.0005 ppm
Average Eu mass fraction measured in the graphite sphere	0.0003116 ppm
Minimum Eu mass fraction measured in the graphite sphere	0.0002 ppm
Maximum Sm mass fraction measured in the graphite sphere	0.0190 ppm
Average Sm mass fraction measured in the graphite sphere	0.003233 ppm
Minimum Sm mass fraction measured in the graphite sphere	0.002 ppm
Cross section of the activation reaction of Eu-151 (n, γ) Eu-152	9204 b
Cross section of the activation reaction of Eu-152 (n, γ) Eu-153	12,800 b
Cross section of the activation reaction of Eu-153 (n, γ) Eu-154	312 b
Cross section of the activation reaction of Eu-154 (n, γ) Eu-155	1340 b
Cross section of the activation reaction of Sm-152 (n, γ) Sm-153	206 b
Cross section of the activation reaction of Sm-153 (n, γ) Sm-154	420 b

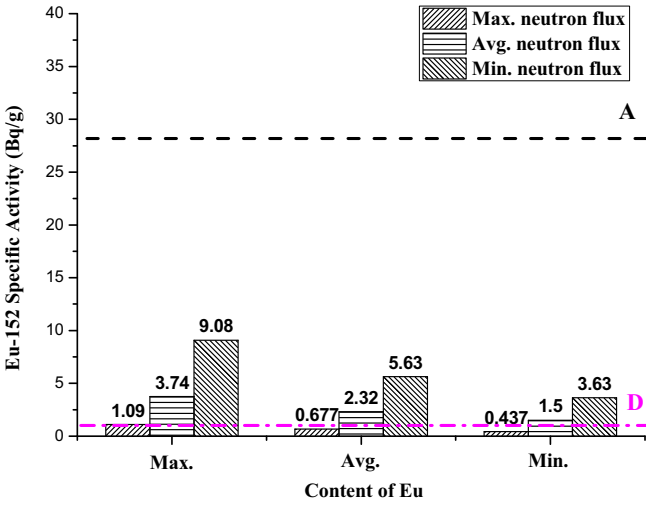

Fig. 15. Comparison of calculated Eu-152 specific activities based on different contents of Eu (maximum, average and minimum) with average experimental values from irradiated graphite spheres A and D.

$$\frac{dN_{G\_Eu-153}}{dt} = -\sigma_{Eu-153}\phi_{Th}N_{G\_Eu-153} \tag{26}$$

$$\frac{dN^{G\_Sm-152}_{Eu-154}}{dt} = \sigma_{Eu-153}\phi_{Th}N^{Sm-153}_{Eu-153} - \sigma_{Eu-154}\phi_{Th}N^{G\_Sm-152}_{Eu-154} - \lambda_{Eu-154}N^{G\_Sm-152}_{Eu-154} \tag{27}$$

$$\frac{dN^{Sm-153}_{Eu-153}}{dt} = -\sigma_{Eu-153}\phi_{Th}N^{Sm-153}_{Eu-153} + \lambda_{Sm-153}N^{G\_Sm-152}_{Sm-153} \tag{28}$$

$$\frac{dN^{G\_Sm-152}_{Sm-153}}{dt} = \sigma_{Sm-152}\phi_{Th}N_{G\_Sm-152} - \sigma_{Sm-153}\phi_{Th}N^{G\_Sm-152}_{Sm-153} - \lambda_{Sm-153}N^{G\_Sm-152}_{Sm-153} \tag{29}$$

$$\frac{dN_{G\_Sm-152}}{dt} = -\sigma_{Sm-152}\phi_{Th}N_{G\_Sm-152} \tag{30}$$

where $N^{G\_Eu-153}_{Eu-154}$ and $N^{G\_Sm-152}_{Eu-154}$ are the numbers of Eu-154 atoms generated by activation reactions of natural Eu-153 and chain reaction of natural Sm-152 in the graphite sphere respectively, N_{G_Eu-153} and N_{G_Sm-152} are the number of Eu-153 and Sm-152 atoms in the graphite sphere separately, N^{Sm-153}_{Eu-153} and $N^{G\_Sm-152}_{Sm-153}$ are the number of Eu-153 and Sm-153 atoms produced from chain reaction of natural Sm-152 in the graphite sphere individually, σ_{Eu-153} and σ_{Eu-154} are the cross sections of the activation reactions of Eu-153 (n, γ) Eu-154 and Eu-154 (n, γ) Eu-155 (b) respectively, σ_{Sm-152} and σ_{Sm-153} are the cross sections of the activation reactions of Sm-152 (n, γ) Sm-153 and Sm-153 (n, γ) Sm-154 (b) separately, and, λ_{Eu-154} and λ_{Sm-153} are the decay constants of Eu-154 and Sm-153 (s^{-1}) individually.

According to parameters about Eu-153 and Sm-152 listed in Tables 11 and 12 provides the specific activity calculation results of Eu-154 based on different parameters combination of neutron flux and measured Eu-153 and Sm-152 mass fractions in the graphite sphere. Assuming the irradiated graphite spheres experienced 225 EFPDs, the specific activity of Eu-154 shows a much larger change with the variation of Eu-153 and Sm-152 mass fractions than with the variation of neutron flux. Especially the measured Sm mass fraction values in the sampling batches of the graphite spheres change from 0.0020 ppm to 0.0190 ppm, the specific activities of Eu-154 vary from 17.5 Bq/g to 166 Bq/g accordingly with the average neutron flux. While the measured

Table 12
Specific activity calculation results of Eu-154 with different parameters at 225 equivalent full power operation days.

Item		Specific activity of Eu-154 (Bq/g)		
		Flux		
		Maximum	Average	Minimum
Eu (Eu-153)	Maximum	1.18E+02	1.09E+02	9.96E+01
	Average	7.31E+01	6.73E+01	6.18E+01
	Minimum	4.71E+01	4.34E+01	3.98E+01
Sm (Sm-152)	Maximum	2.32E+02	1.66E+02	1.27E+02
	Average	3.79E+01	2.82E+01	2.16E+01
	Minimum	2.35E+01	1.75E+01	1.34E+01

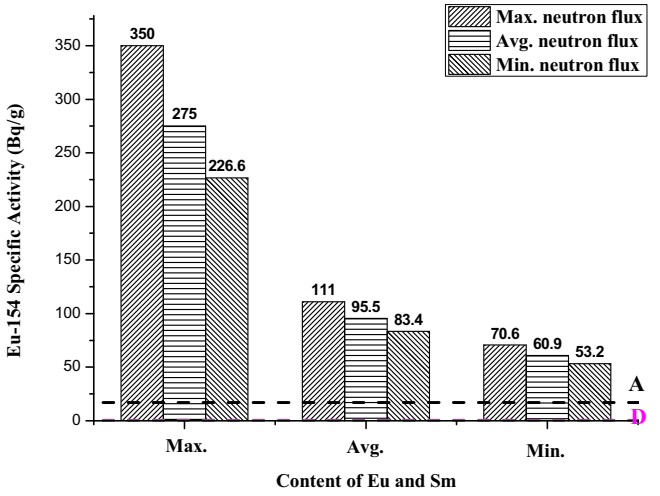

Fig. 16. Comparison of calculated Eu-154 specific activities based on different contents of Eu and Sm (maximum, average and minimum) with average experimental values from irradiated graphite spheres A and D.

Eu mass fraction values in the sampling batches of graphite spheres vary in a small range, from 0.0002 ppm to 0.0005 ppm, also the specific activities of Eu-154 change very little.

Fig. 16 exhibits theoretical calculations of Eu-154 specific activity in comparison with the average experimental values measured in the irradiated graphite spheres A and D. The calculated values cover the experimental values reasonably. Unlike the generation mechanism of Eu-152, the Eu-154 can be produced not only by the activation reaction of natural europium but also by the activation reaction from natural samarium. Therefore, both the Eu mass fraction and the Sm mass fraction in the graphite can have significant effects on the specific activity of Eu-154 in the irradiated graphite sphere of HTR-10.

5. Discussion

Based on experimental results of four irradiated graphite spheres, we concluded that source terms are determined by the long lived nuclides H-3, C-14, Co-60, Cs-137, Eu-152, and Eu-154 in the matrix graphite of fuel elements and graphite spheres of HTR-10. The surface γ dose rates strongly depend on the specific activities of Co-60 in irradiated graphite spheres. The average total β counting rate per gram indicates a close relationship with the specific activity of Co-60, though the specific activities of H-3 and C-14 are higher in some irradiated graphite spheres. Therefore, the Co-60 is a characteristic nuclide to represent the radioactive level of irradiated graphite spheres of HTR-10 with a preliminary

measurement of the surface γ dose rate and the total β counting rate per gram.

Compared with the experimental data available about specific activities of key nuclides in the graphite of AVR, it seems that the average radioactive level in the matrix graphite of HTR-10 operating elements is much lower. Measurements taken on AVR graphites are listed in Table 13. On one hand, this can be explained that the AVR reactor has been operated for a long time with higher thermal power and several types of fuel elements including bistructural-isotropic (BISO) coated particles had been used, which greatly promoted the transport and release of radioactive nuclides in the reactor core. On the other hand, the high core release has caused fission product profiles with a strong decreasing gradient of all nuclide concentrations from the sphere surface towards the inside showing that the contamination comes from the outside (IAEA, 1997). In contrast, the primary loop of HTR-10 shows a rather low radioactive contamination level up to now and the TRISO coated particles in the fuel elements exhibit a good performance on the retention ability of fission products. Besides, the contamination with uranium in the HTR-10 spheres appears to be lower compared to AVR spheres according to the fission gas release observations during the irradiation experiment HFR-EU1 which contained fuel spheres from both Chinese and German production (IAEA, 2012). Also, the content of impurities in the matrix graphite of HTR-10 may be lower than those of AVR based on the comparison of activation products.

The experimental results in the graphite spheres B and C show a nearly symmetric distribution of radioactive nuclides in the graphite relative to the center. All the nuclides show a nearly homogenous specific activities distribution inside the graphite spheres. Only at the surface, the change of the concentration occurs. This can be understood that H-3, C-14, Co-60, Eu-152, and Eu-154 in the irradiated graphite sphere of HTR-10 are mainly generated from the activation of impurities in the graphite which possess nearly even distributions due to the manufacturing process (Tang et al., 2002). Cs-137, as a typical fission product, is considered to be produced by the fission reaction of uranium in the matrix graphite. Thus, a homogenous distribution in the interior of the irradiated graphite sphere of HTR-10 is given as expected. Since the surface of the irradiated graphite sphere is the interface between the matrix graphite and primary coolant or other materials, adsorption, desorption, absorption, and diffusion processes may happen, which can lead to a concentration alteration as observed in the experimental results. However, these physical and chemical processes depend on the characteristics of individual nuclides, the concentration of each nuclide in the matrix graphite and in the primary helium, the ambient conditions for the graphite spheres, the operational history of the reactor, etc. For H-3, the specific activities are clearly higher at the surface than those in the interior of graphite spheres B, C and D, while it is not very clear in graphite sphere A. It can be easily understood that matrix graphite acts as a sink for tritium since the absorption interaction between tritium and graphite is strong (Tsetskhladze et al., 1988; Xie et al., 2017). However, in graphite sphere A, the specific activity of H-3 is rather large, the sorption effect of H-3 is not as clearly visible as in graphite spheres B, C and D. For C-14, the specific activities are slightly higher at the surface than those in the interior of graphite spheres A, B, C and D. Compared with the experimental results observed in the matrix graphite of AVR (Wenzel et al., 1979), the higher concentration of C-14 at the surface can be explained that most of the air is stored in the surface layer when fresh fuel spheres are loaded. However, unlike a steep increase of C-14 concentration at the surface of the fuel element in AVR, the content of N impurities in the surface layer of HTR-10 graphite spheres may be much lower, resulting in a slight higher concentration of C-14 at the surface.

The specific activities of Co-60 in graphite spheres A, B and D at the surface are clearly higher than those in the interior, while the distribution of Co-60 in the graphite sphere C is rather equal, even at the surface. In HTRs, the Co-60 is generated from the activation reactions of Co-59 and Ni-60. However, the contents of impurities exhibit a large variation among individual graphite spheres from different sampling batches. Therefore, the specific activity of Co-60 in different irradiate graphite spheres could change significantly. Due to the abrasion and friction, the surface of the graphite sphere with lower Co-60 specific activity can be adhered by substances (graphite dust, etc.) from other graphite spheres and/or fuel elements with higher Co-60 specific activity. This process can increase the Co-60 concentration at the surface for the irradiate graphite spheres A, B and D. For Cs-137, the specific activities in all measured irradiated graphite spheres are rather low, and it is not very clear to quantify the variation tendency of specific activities at the surface. Since only in graphite spheres A and D, the specific activities of Eu-152 and Eu-154 were determined, the distributions of Eu-152 and Eu-154 in the irradiated graphite spheres are nearly equal due to the generation from activation reaction of impurities in the graphite.

As indicated above, in the irradiated graphite spheres of HTR-10, the dominant sources of H-3, C-14, Co-60, Eu-152 and Eu-154 are the activation reaction of Li-6, the activation reactions of C-13 and N-14, the activation reaction of Co-59, the activation reactions of Eu-151, and the activation reactions of Eu-153 and Sm-152, respectively. The specific activity of Cs-137 in the irradiated graphite spheres of HTR-10 mainly depends on the free uranium contamination in the graphite. By now the measured uranium contamination fractions in the graphite spheres of HTR-10 are all less than the design value which was adopted in the Final Safety Analysis Report of HTR-10. Based on the sensitivity analysis, we can see that the content of impurities in the matrix graphite can make significant effects on the activity of activation products in the graphite sphere of HTR-10, in comparison with variation of the neutron flux in the reactor. The content of impurities varies with different sampling batches of graphite spheres (Zhao et al., 2006). However, all the measured values of impurities available are less than those designed values in HTR-10 if the designed value for the specific element has been set, which is the case for Li, B and Ni mass fractions in the matrix graphite of HTR-10. This indicates that the radioactive assessment for the primary loop of HTR-10 based on design values will be sufficiently conservative. In future, the designed values for Co, Eu and Sm mass fractions can also be proposed for

Table 13
Experimental specific activities of typical nuclides in the graphite materials of AVR.

Item	Nuclides	Specific activities (Bq/g)
AVR core graphite (Bisplinghoff et al., 2000)	H-3	1.2×10^6
	C-14	6.3×10^4
	Co-60	4.1×10^5
	Cs-137	4.4×10^3
	Eu-152	<150
	Eu-154	9.7×10^3
AVR irradiated fuel sphere (Reitsamer et al. 1987)	Co-60	2.4×10^4
	Cs-137	2.8×10^4
	Eu-154	1.1×10^3
AVR reflector graphite (Fachinger et al., 2008)	H-3	8.8×10^5
	C-14	9.5×10^4
	Co-60	2.7×10^4
	Cs-137	1.9×10^3
	Eu-154	560
AVR graphite dust (Gottaut and Krüger, 1990)	Co-60	2.0×10^5–8×10^6
	Cs-137	2×10^6–9.6×10^7
Matrix graphite of the AVR fuel element (Wenzel et al., 1979)	C-14	3.7×10^4

the matrix graphite of fuel elements and graphite spheres, which may effectively limit the amount of activation products in the core of HTGRs.

6. Conclusion

Totally four irradiated graphite spheres from the reactor core of HTR-10 have been studied experimentally with previously developed experimental methods, including the total β counting measurement with a total α/β analyzer, and the specific activities measurement for γ nuclides with a high-purity germanium detector connected to a multichannel analyzer and for β nuclides with a liquid scintillation counter. Source terms in the irradiated graphite spheres have been determined explicitly, and the key nuclides were identified as H-3, C-14, Co-60, Cs-137, Eu-152, and Eu-154. The specific activities of these key nuclides show a rather symmetric distribution relative to the center of the graphite sphere, and are nearly homogeneous in the interior of the graphite sphere. The total β counting rate per gram, as well as the surface γ dose rate of the irradiated graphite spheres are dominated by the specific activity of Co-60. The specific activities for each nuclide in the four irradiated graphite spheres exhibit large differences individually except for those of Cs-137 which is thought to be generated from the fission reaction of uranium in the graphite.

A sensitive analysis of source terms in the irradiated graphite sphere of HTR-10 has been provided considering the following factors: the design value and the measured range of the content of impurities in the matrix graphite, the range of the neutron flux in the reactor core, the measured and estimated natural uranium contamination fraction in the graphite sphere, and the variation of dwell time for the graphite spheres in the core. It indicates that the content of impurities in the graphite plays an important role in the specific activity of key nuclides in the irradiated graphite spheres of HTR-10. In comparison with the measurements, the dominant source of H-3 in the irradiated graphite sphere of HTR-10 is the activation reaction of Li-6. The second contributor of H-3 in the matrix graphite is the activation reaction of B-10. The specific activity of C-14 in a graphite sphere can be greatly affected by the actual content of N-14 in the matrix graphite. Most of the Co-60 in the irradiated graphite spheres of HTR-10 comes from the activation of Co-59. To strictly control the content of Co-59 in the graphite matrix is very meaningful to decrease the γ radiation dose rate in HTR-10. The calculations of the specific activity of Cs-137 in the irradiated graphite spheres of HTR-10 based on the estimated and measured natural uranium contamination agrees well with the experimental observations. The Eu-152 is thought to be generated from the activation reaction of Eu-151. The calculations of the specific activities of Eu-152 can be compared with experimental data. However, the calculated specific activities of Eu-154 in the irradiated graphite sphere of HTR-10, which is produced by the activation reactions of Eu-153 and Sm-152, are a little higher than the experimental observations. The control of the contents of Eu and Sm in the graphite matrix is also an issue to be considered in waste minimization of HTGRs.

The current research can supply important information for the source term analysis, waste minimization, decommissioning work of HTR-10, and improve knowledge of behavior of fission products and activation products in HTGRs.

Acknowledgements

This work was supported by the National Natural Science Foundation of China (No. 11575099), the Tsinghua University Initiative Scientific Research Program (No. 20151080375), the Chinese National S&T Major Project (Grant No. ZX069), and the Major National R&D Projects (2013ZX06002001-014). We are grateful for the fruitful discussions with Dr. Bing Xia, Mr. Liqiang Wei, Mr. Jianzhu Cao, Prof. Bing Liu, Prof. Chunhe Tang, Prof. Fu Li, and Prof. Yuanzhong Liu in INET, Tsinghua University, Beijing, China.

References

Bäumer, R., Barnert, H., 1990. AVR-Experimental High-Temperature Reactor: 21 Years of Successful Operation for a Future Energy Technology. The Association of German Engineers (VDI-Verlag GmbH), Düsseldorf, Germany.

Bisplinghoff, B., Lochny, M., Fachinger, J., Brüchner, H., 2000. Radiochemical characterization of graphite from Jülich experimental reactor (AVR). Nuclear Energy 39, 311–315.

Davis Jr., W., 1977. Carbon-14 Production in Nuclear Reactors. Oak Ridge National Lab. ORNL/NUREG/TM-12.

Fachinger, J., Lensa, W.N., Podruhzina, T., 2008. Decontamination of nuclear graphite. Nucl. Eng. Des. 238, 3086–3091.

Gainey, B.W., 1976. A Review of Tritium Behavior in HTGR Systems. GA-A13461. General Atomic Company.

Gottaut, H., Krüger, K., 1990. Results of experiments at the AVR reactor. Nucl. Eng. Des. 121, 143–153.

IAEA, 1997. Fuel performance and fission product behaviour in gas-cooled reactors. IAEA-TECDOC-978.

IAEA, 2012. Advances in high temperature gas cooled reactor fuel technology. IAEA-TECDOC-CD-1674.

Kissane, M.P., 2009. A review of radionuclide behavior in the primary system of a very-high-temperature reactor. Nucl. Eng. Des. 239, 3076–3091.

Lahiri, S., Roy, K., Bhattacharya, S., Maji, S., Basu, S., 2005. Separation of ^{134}Cs and ^{152}Eu using inorganic ion exchangers, zirconium vanadate and ceric vanadate. Appl. Radiat. Isot. 63, 293–297.

Li, H., Liu, X., Xie, F., Jia, F., 2017. Experimental study on the content and distribution of key nuclides in an irradiated graphite sphere of HTR-10. Nucl. Eng. Des. 323, 39–45.

Liu, X., Huang, X., Xie, F., Jia, F., Feng, X., Li, H., 2017. Source term analysis of irradiated graphite in the core of HTR-10. Sci. Technol. Nucl. Inst. (2017) 2614890 (1–6).

Morris, R.N., Kissane, M.P., Petti, D., Powers, D., Wichner, R., 2008. Next generation nuclear plant phenomena identification and ranking tables (PIRTs): fission product transport and dose PIRTs. US NRC, NUREG/CR-6944, vol. 3.

Nichols, A.L., Aldama, D.L., Verpelli, M., 2008. Handbook of nuclear data for safeguards: database extensions. International Atomic Energy Agency, INDC (NDS)-0534.

Niese, S., Gleisberg, B., 1996. Determination of radioisotopes of Ce, Eu, Pu, Am and Cm in low-level wastes from power reactors using low-level measuring techniques. Appl. Radiat. Isot. 47, 1113–1114.

Reitsamer, G., Zeger, J., Serro, W., Falta, G., 1987. Nachbestrahlungsuntersuchungen an den AVR-Brennelementen 70/26 und 70/32, Report OEFZS-A-1105, Österreichisches Forschungszentrum Seibersdorf.

Smith, D., Woods, D.H., Makepeace, J.L., Mercer, R.A., Downey, C.W.A., 1992. Standardisation of ^{125}Sb and ^{154}Eu, and measurement of absolute gamma-ray emission probabilities. Nucl. Instr. and Meth. A312, 353–358.

Tang, C., Tang, Y., Zhu, J., Zou, Y., Li, J., Ni, X., 2002. Design and manufacture of the fuel element for the 10 MW high temperature gas-cooled reactor. Nucl. Eng. Des. 218, 91–102.

Tsetskhladze, T.V., Cherkzishvili, L.I., Chikhladze, L.A., 1988. Interaction of tritium with graphite. Soviet At. Energy 64 (3), 254–258.

U.S. DOE Nuclear Energy Research Advisory Committee (NERAC) and the Generation IV International Forum (GIF), 2002. A technology roadmap for generation IV nuclear energy systems. GIF-002-00.

Vimalnath, K.V., Das, M.K., Ananthakrishnan, M., Ramamoorthy, N., 2005. Facile access to ^{154}Eu, a new reference source for calibration in gamma ray spectrometry. Appl. Radiat. Isot. 62, 17–23.

Wang, S., Xie, F., Li, H., Cao, J., Li, F., Wei, L., 2015. Study on the production mechanism of Co-60 in the primary loop of HTR-10. In: Proceedings of 23rd International Conference on Nuclear Engineering, Chiba, Japan.

Wei, L., Xie, F., Chen, X., Ma, T., Tong, J., Li, F., 2016. Summary and experience feedback on the restart and power operation after a long-time shutdown of HTR-10. In: Proceeding of the 8th International Topical Meeting on High Temperature Reactor Technology (HTR 2016), Las Vegas, NV, USA.

Wenzel, U., Herz, D., Schmidt, P., 1979. Determination of ^{14}C in spent HTGR fuel elements. J. Radioanal. Chem. 53 (1–2), 7–15.

Wichner, R.P., Dyer, F.F., 1980. Carbon-14 Production in the Peach Bottom HTGR Core. Oak Ridge National Lab. ORNL-5597.

Wu, Z., Lin, D., Zhong, D., 2002. The design features of the HTR-10. Nucl. Eng. Des. 218, 25–32.

Xie, F., Cao, J., Chen, Z., Dong, Y., 2015. The design and study of the radioactive graphite dust experimental system in the primary loop of the HTR-10. At. Energy Sci. Technol. 49 (4), 744–749 (in Chinese).

Xie, F., Cao, J., Feng, X., Liu, X., Tong, J., Wang, H., Dong, Y., Zhang, Z., Loyalka, S.K., 2017. Experimental research on the radioactive dust in the primary loop of HTR-10. Nucl. Eng. Des. 324, 372–378.

Xie, F., Cao, J., Feng, X., Tong, J., Dong, Y., Zhang, Z., Scarlat, R., 2018. Study of tritium in the primary loop of HTR-10: experiment and theoretical calculations. Prog. Nucl. Energy 105, 99–105.

Xu, Y., Li, H., Xie, F., Cao, J., Tong, J., 2017. Source term analysis of tritium in HTR-10. Fusion Sci. Technol. 71, 671–678.

Zhang, Z., Wu, Z., Wang, D., Xu, Y., Sun, Y., Li, F., Dong, Y., 2009. Current status and technical description of Chinese 2×250MWth HTR-PM demonstration plant. Nucl. Eng. Des. 239, 1212–1219.

Zhao, H., Liang, T., Zhang, J., He, J., Zou, Y., Tang, C., 2006. Manufacture and characteristics of spherical fuel elements for the HTR-10. Nucl. Eng. Des. 236, 643–647.